

## An Operational Method for Separating Wind Sea and Swell from Ocean Wave Spectra\*

DAVID W. WANG AND PAUL A. HWANG

*Oceanography Division, Naval Research Laboratory, Stennis Space Center, Mississippi*

(Manuscript received 13 October 2000, in final form 30 May 2001)

### ABSTRACT

Coexistence of wind sea generated locally and swell radiated from distant storms often results in double-peaked or multiple-peaked spectra. Identification and separation of the wave energies of wind sea and swell provide a more realistic description of the sea state, which is of great importance to scientific and engineering applications. This paper describes a method based on the peak frequency of a newly defined steepness function to separate the wave energies of wind sea and swell from the omnidirectional wave spectra. This steepness method does not rely on the availability of the information of wind velocities and wave directions and can be easily implemented for operational uses. Verification results using directional wave data collected from buoys in the Gulf of Mexico and offshore California are presented.

### 1. Introduction

As sea states consist of local wind-generated waves and swells of distant storms, the wave energy spectra often show two or more spectral peaks corresponding to different generation sources. The probability of occurrences of double-peaked spectra are reportedly in the range of 10%–30% (Aranuvachapun 1987; Guedes Soares 1991). Depending on sea states and measurement sites, the occurrence of double-peaked spectra could be even higher. The coexisting of wind sea and swell can significantly affect sea-keeping safety, offshore structure designs, small boat operations and ship passages over harbor entrance, and surf forecasting (Earle 1984). The mixed seas also affect the dynamics of near-surface processes such as air–sea momentum transfer (Dobson et al. 1994; Donelan et al. 1997; Mistuyasu 1991, 1997; Hanson and Phillips 1999). Identification and separation of wave components of wind sea and swell provide a more realistic depiction of the sea state and is of great importance and interest to both scientific and engineering applications.

Most methods for the automatic identification and separation of wave components of wind sea and swell rely on the determination of a separation frequency  $f_s$

for a given wave spectrum. Wave components at frequencies higher than  $f_s$  are generated by local winds and wave components at frequencies lower than  $f_s$  are from swell. Assuming the separation frequency is linearly related to the spectral peak of a wind sea, Earle (1984) proposes an empirical relation between the separation frequency and the local wind speed  $U$  based on the Pierson–Moskowitz (PM) spectral model (Pierson and Moskowitz 1964). The relation can be expressed as

$$f_s = \frac{\beta}{U}, \quad (1)$$

where  $f_s$  is in hertz,  $U$  is in meters per second, and  $\beta$  is an empirical constant. A very similar relation is also derived by assuming that the deep-water phase velocity of wind-generated wave components is less than wind speed (The WAMDI Group 1988; Dobson et al. 1994). Using both wind and wave directional data, a directional spectra partitioning scheme has been developed for identifying wind sea and tracking storm sources (Gerling 1992; Kline and Hanson 1995; Hanson 1996; Hanson and Phillips 2001).

A more desirable approach is to determine a separation frequency between the wind sea and swell peaks from a given spectrum alone (Vartdal and Barstow 1987). Wind sea and swell peaks can mix with spectral irregularities, which are the local maximums in wave spectrum resulting from artifacts of random processes. Identification of wind sea and swell peaks from the spectral irregularities is not always very reliable. Using an empirically determined width of the confidence intervals of the spectral data, a procedure is developed by Rodriguez and Guedes Soares (1999) to differentiate the

\* U.S. Naval Research Laboratory Contribution Number JA/7330-00-0036.

Corresponding author address: Dr. David Wang, Oceanography Division, Naval Research Laboratory, Stennis Space Center, MS 39529.

E-mail: dwang@nrlssc.navy.mil

legitimate energy peaks of wind sea and swell from the spectral irregularities caused by the artifacts of random processes. Similar methods are also proposed by Guedes Soares (1984) and Guedes Soares and Nolasco (1992). These peak identification methods require a priori knowledge of the degree of freedom (DOF) of spectral data and have to inefficiently examine every local maximum. The empirical peak identification algorithm based on DOF also lacks physical basis of wind wave generation and can easily result in misidentifications of wind sea and swell peaks, especially for spectra with multiple strong swell peaks.

The purpose of this study is to develop a physics-based method to separate energies of wind sea and swell from wave spectra without the need of wind and directional wave information. Section 2 describes the development of the method. Field data testing of the method is shown in section 3. Section 4 presents examples of applying the separation method to characterize wave climate with the wave heights and wave periods of the wind sea and swell components. A summary is given in section 5.

**2. Development of the steepness method**

For a random wave field, the average steepness of wave components above a given frequency  $f_*$  can be described by the ratio between the representative wave height and the wavelength. This ratio is a frequency-dependent steepness function,  $\alpha(f_*)$  expressed as

$$\alpha(f_*) = \frac{H_*}{L_*}, \tag{2}$$

where  $H_*$  and  $L_*$  are, respectively, the representative wave height and wavelength for wave components above  $f_*$ . Using the linear dispersion relation, the wavelength can be related to a representative wave period  $T_*$  by

$$L_* = \frac{gT_*^2}{2\pi}, \tag{3}$$

where  $g$  is the gravitational acceleration. The representative wave height and wave period are defined as

$$H_* = 4\sqrt{m_{0*}}, \text{ and} \tag{4}$$

$$T_* = \sqrt{\frac{m_{0*}}{m_{2*}}}, \tag{5}$$

where  $m_{0*}$  and  $m_{2*}$  are the spectral moments computed by

$$m_{n*}(f_*) = \int_{f_*}^{f_{\max}} f^n S(f) df, \quad n = 0, 2, \tag{6}$$

where  $S(f)$  is the omnidirectional wave spectrum and  $f_{\max}$  is the upper-frequency limit of  $S(f)$ . As  $f_*$  reaches the lower-frequency limit  $f_{\min}$  of  $S(f)$ ,  $H_*$  and  $T_*$  are,

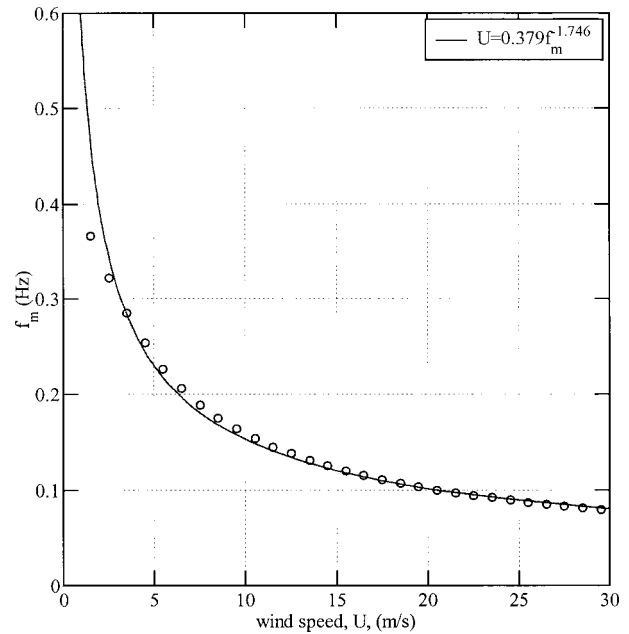


FIG. 1. Wind speed vs peak frequency  $f_m$  of the steepness function based on the PM spectral model (circles). The solid line represents the curve-fitting result by regression analysis [see Eq. (8)].

respectively, the commonly used significant wave height and average zero-up-crossing wave period. The value of  $\alpha(f_{\min})$  then is the significant steepness (Tucker 1991, p. 97), which is also referred to as the significant slope by Huang et al. (1981). Substituting (3), (4) and (5) into (2), the steepness function can be expressed as

$$\alpha(f_*) = \frac{8\pi \left[ \int_{f_*}^{f_{\max}} f^2 S(f) df \right]}{g \left[ \int_{f_*}^{f_{\max}} S(f) df \right]^{0.5}}. \tag{7}$$

The steepness function in (7) is derived using the integral property of the wave spectrum, which smoothens out most spectral irregularities due to artifacts of random processes. Compared to the spectral peak  $f_p$ , the peak frequency of the steepness function  $f_m$  is less affected by the spectral irregularities. Because of the  $f^2$  factor in the calculation of the steepness function, the characteristics of the steepness function and its peak frequency are more related to high-frequency waves of the wind sea. The additional swell energies at lower frequencies could not significantly change the characteristics of the steepness function and its peak frequency.

Using the PM spectral model to represent  $S(f)$ , the steepness function for the spectra of various wind speeds are computed from (7). An upper-frequency limit  $f_{\max} = 0.5$  Hz is used. Figure 1 shows the close relation between the peak frequency of the steepness function  $f_m$  and the wind speed  $U$ . The peak frequency decreases as the wind speed increases, which can be approximated by

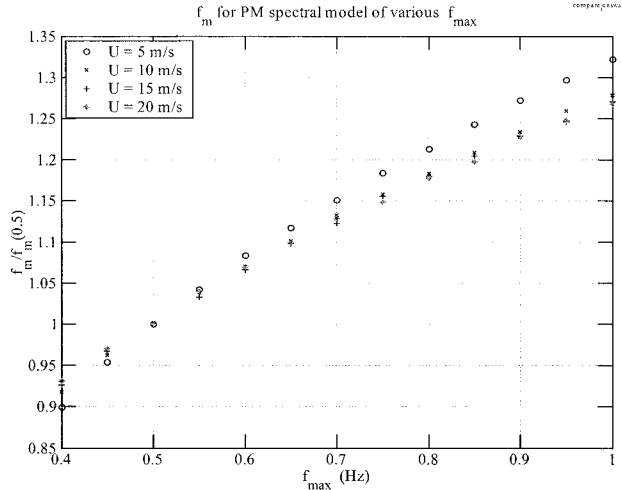


FIG. 2. The normalized peak frequency  $f_m$  of the steepness function vs the upper-frequency limit  $f_{max}$  for the PM spectral model of wind speeds 5, 10, 15 and 20  $m s^{-1}$ .

$$U = a(f_m)^b, \tag{8}$$

where  $U$  is in  $m s^{-1}$  and  $f_m$  is in  $Hz$ ,  $a = 0.379$  and  $b = -1.746$  are two empirical constants determined from the regression analysis.

The effect of different upper-frequency limit  $f_{max}$  to the peak frequency of the steepness function is further examined for the PM spectral model for wind speeds 5, 10, 15, and 20  $m s^{-1}$  with the upper-frequency limit  $f_{max}$  varying from 0.4 to 1.0 Hz. Figure 2 shows the normalized peak frequency  $f_m$  of the steepness function of the PM spectra versus  $f_{max}$ . In this plot,  $f_m$  for a different upper-frequency limit is normalized by  $f_m$  for  $f_{max} = 0.5$  Hz. The peak frequency  $f_m$  increases as  $f_{max}$  increases. For example, at 5  $m s^{-1}$  wind speed, the peak frequency  $f_m$  increases by about 33% as  $f_{max}$  increases from 0.5 to 1.0 Hz. For most operational wave measurement systems, the upper-frequency limit is usually within 0.4 to 0.6 Hz. In this range, the variation of the peak frequency  $f_m$  with respect to  $f_m$  at  $f_{max} = 0.5$  is less than 10%.

Considering that local wind-generated waves should have its phase velocity  $C$  less than wind speed  $U$ , the separation frequency of wind sea and swell is the frequency  $f_s$  with its phase velocity  $C_s$  satisfying the relation,  $C_s = U$ , where subscript  $s$  represents the properties related to the separation frequency. Using the deep-water-phase velocity,  $C = g/2\pi f$ , the separation frequency is related to wind speed by

$$f_s = \frac{g}{2\pi U}. \tag{9}$$

Substituting (8) into (9), the relation between  $f_s$  and  $f_m$  can be expressed as

$$f_s = A(f_m)^B, \tag{10}$$

where  $A = 4.112$  and  $B = 1.746$ . The separation fre-

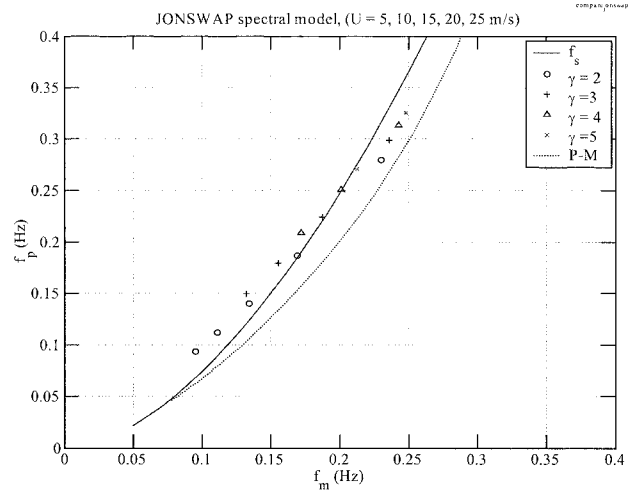


FIG. 3. The peak frequency  $f_m$  of the steepness function vs the peak frequency of the simulated JONSWAP spectra for various wind speeds  $U$  and peak enhancement factors  $\gamma$ . The solid line represents the separation frequency calculated from  $f_m$  based on (10). The dotted line represents the relation of the spectral peak  $f_p$  and  $f_m$  for the PM spectral model of  $U = 5$  to 30  $m s^{-1}$ .

quency can then be determined from the peak frequency of the steepness function without the use of wind speed.

The relation in (10) is developed based on (8) using the PM spectral model of fully developed seas. Applying (10) to spectra of younger seas is examined here. For spectra of various young sea states, the Joint North Sea Wave Project (JONSWAP) spectral model is simulated for wind speed  $U = 5, 10, 15, 20,$  and  $25 m s^{-1}$  with the peak enhancement factor  $\gamma = 2, 3, 4,$  and  $5$ . The shape parameters of the JONSWAP spectral model for given  $U$  and  $\gamma$  are calculated based on the relations proposed by Lewis and Allos (1990). The steepness function and the separation frequency  $f_s$  for the simulated JONSWAP spectra are calculated respectively from (7) and (10). Because the upper-frequency limit  $f_{max} = 0.5$  Hz is used for the steepness function in (7), we only use the simulated JONSWAP spectra with its peak frequency  $f_p$  less than 0.4 Hz. Figure 3 shows the spectral peak  $f_p$  versus the peak frequency  $f_m$  of the steepness function for the selected JONSWAP spectra. The solid line represent the separation frequency calculated from  $f_m$  based on (10) for the simulated JONSWAP spectra, which is very close to the spectra peaks of the simulated JONSWAP spectra. The dotted line represents the relation of the spectral peak  $f_p$  and  $f_m$  for the PM spectral model of wind speed  $U = 5$  to 30  $m s^{-1}$ .

### 3. Field testing of the steepness method

The proposed method is tested under two frequently occurring marine weather conditions of coexisting wind sea and swell. The first condition is related to meteorological frontal passage during which the local wind

has a rapid shift in the wind direction. Following the frontal passage, the newly shifted local wind generates waves over the existing developed waves. The wave spectra often show two distinctive energy peaks associated with the newly generated waves and preexisting developed waves. The second condition usually occurs in coastal areas facing open oceans, where the long-period swell radiated from distant storms coexists with the locally generated wind sea. The period, energy, and arrival time of swell are not related to local wind conditions. The presence of swell often causes significant and unexpected changes to the local sea state. For testing the validity and reliability of the steepness method under these two conditions, we use wind and directional wave data from an offshore buoy in the Gulf of Mexico during the passage of a cold front for the first condition and from an offshore buoy off the California coast for the second condition. Both buoys are deployed and operated by the National Data Buoy Center (NDBC). Directional wave data are estimated from buoy's heave, pitch, and roll motions by an NDBC wave processing module on board the buoys. Wind data are collected by an R. M. Young propeller-type anemometer mounted at the top of the buoy mast at approximately 5 m above the waterline. Details of the wind and wave measurement systems of the NDBC buoys can be found in Steele et al. (1992) and Steele and Mettlach (1993). The wave spectral data has a frequency range of 0.03–0.485 Hz with 24 degrees of freedom (DOFs).

#### a. Mixed seas during a frontal passage

For the condition of mixed seas due to frontal passage, the wind and wave data are collected from a buoy moored off the Alabama coast at a water depth of 29.3 m. Figure 4 shows the time history of the hourly measured wind and wave data from 13 to 14 December 1995. During the first 26 hours, the sea state is dominated by a growing wind sea generated by a long-fetched southeasterly wind over the Gulf of Mexico (Figs. 4a and 4b). As the southeasterly wind increases from 5 to 15 m s<sup>-1</sup>, the significant wave height gradually grows from 0.5 to 4 m with the peak wave period increasing from 4 to 8 s (Figs. 4c and 4d). The peak wave direction generally aligns with the southeasterly wind direction. In the early hours of 14 December, the frontal passage causes a rapid change of the wind direction to the northwest and a decrease of the wind speed to less than 4 m s<sup>-1</sup>. Following the wind direction shift, the significant wave height starts to decay while the northwesterly wind increases to about 10 m s<sup>-1</sup> and remains steady for the rest of period. As the wind direction shifts to the northwest direction following the frontal passage, the peak wave direction still remains southeasterly. Only in the late hours of 14 December, the peak wave direction starts to shift to the northwest direction.

Figure 5 shows the wave spectra (Figs. 5a and 5b) and frequency-dependent mean wave directions (Figs.

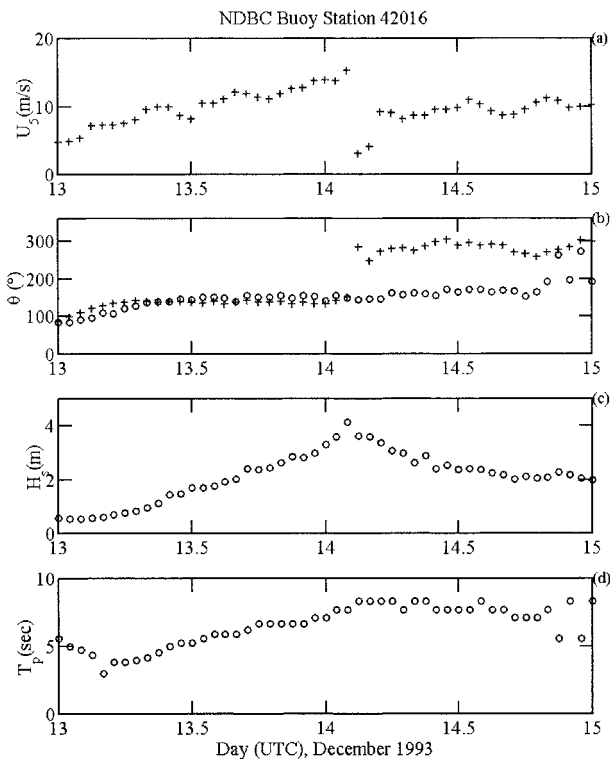


FIG. 4. Time history of hourly measured (a) wind speed, (b) wind direction (crosses) and dominant wave direction (circles), (c) significant wave height, and (d) peak wave period during the period of 13–14 Dec 1993 from the offshore buoy in the Gulf of Mexico (ID 42016).

5c and 5d) at two time periods before the frontal passage. The wind directions are shown as the horizontal dotted lines in Figs. 5c and 5d. The associated steepness functions  $\alpha(f_*)$  of the wave spectra are shown as dotted lines in Figs. 5a and 5b. For the purpose of illustration,  $\alpha(f_*)$  is scaled according to the range of y axis for the wave spectra, such that the maximum value of the scaled  $\alpha(f_*)$  is equal to the half-height of the y axis. The peak frequency of the steepness function is indicated by the vertical dotted lines. The separation frequency from the proposed steepness method (10) is indicated by the vertical dashed lines in Figs. 5a–d. The wave spectrum in Fig. 5b is from the hour of highest significant wave height (4.14 m) and wind speed (15.3 m s<sup>-1</sup>) during the frontal passage period. The wave spectra before the frontal passage are single peaked with their frequency-dependent mean wave directions aligning well with the southeasterly wind direction. The steepness function is much smoother than the wave spectrum with  $\alpha(f_*)$  gradually increases as frequency moves from higher frequencies to lower frequencies. The peak frequency of the steepness function  $f_m$  is very close to the peak frequency of the spectrum  $f_p$ . The separation frequencies are lower than the peak frequencies  $f_p$  and very near the lower-frequency end of the wave spectra. The wave components at frequencies less than the separation fre-

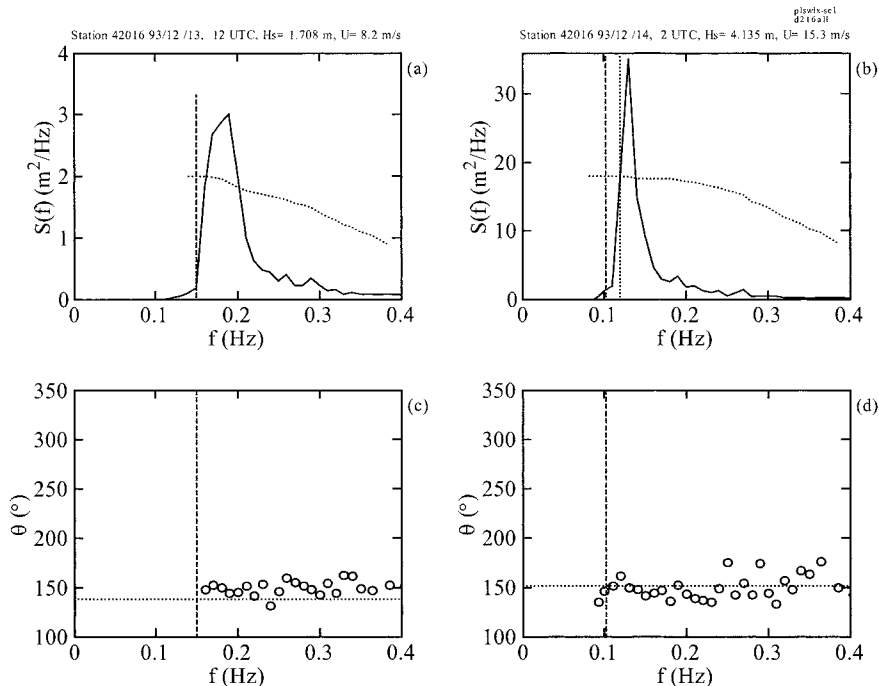


FIG. 5. (a) and (b) Wave spectra and (c) and (d) their respective frequency-dependent mean wave direction (circles) from the offshore buoy in the Gulf of Mexico at two time periods before the frontal passage. The local wind direction is indicated by the horizontal dotted lines in (c) and (d). The dotted lines in (a) and (b) are the scaled steepness function with its peak frequency  $f_m$  indicated by the vertical dotted lines. The vertical dotted line indicates the separation frequency from the steepness method  $f_s$ . Note that  $f_m$  equals  $f_s$  in (a), which causes the overlap of the vertical dotted and dashed lines.

quency have very little energy. This implies that, in practice, the wave spectrum is completely dominated by the wind sea from the southeasterly wind. Similar results are also observed in the period prior to the frontal passage.

Figure 6 shows the wave spectra and frequency-dependent mean wave direction at two time periods after the frontal passage. As the waves generated by the newly shifted northwesterly wind coexist with waves by the earlier southeasterly wind, the wave spectra display two major energy peaks corresponding to the two generation sources. Unlike the double-peaked wave spectra, the steepness functions (dotted lines) remain single peaked with their peak frequencies closer to the high-frequency spectral peak of the northwesterly wind waves. The separation frequency  $f_s$  derived from the steepness method (10) is located between the two spectral peaks (vertical dashed lines). The mean wave directions at frequencies higher than  $f_s$  align with the newly shifted northwesterly wind direction (dotted lines) and those at frequencies lower than  $f_s$  remains in the southeasterly wind direction prior to the frontal passage. The separation frequency from the steepness method shows a proper separation of the wave components by two different generation sources following the frontal passage. Examinations on the wave spectra from the rest of the period after the frontal passage also show the same result.

#### b. Mixed seas with swell from distant storms

For the condition of mixed seas due to swell from distant storms, the wind and wave data are collected from a buoy moored off the California coast at a water depth of approximately 300 m. Figure 7 shows the time history of buoy wind and wave data from a 3-day period (12–14 Dec 1995). In the first 24 hours, the wind speed increases from 5 to 15  $\text{m s}^{-1}$  as the wind direction remains southeasterly. As the wind starts a gradual shift toward northwest at earlier hours of 13 December, the wind speed drops to 1  $\text{m s}^{-1}$  at midday of 13 December and increase to 10  $\text{m s}^{-1}$  at the end of the day. For the most part of 14 December, the wind speed varies between 10 to 12  $\text{m s}^{-1}$  as the wind direction remains northwesterly. Due to the constant arrival of strong westerly swells with peak periods of 12 to 15 s (Figs. 7b and 7d), the variation of sea state deviates significantly from the local wind conditions. As the wind speed decreases from 15 to 1  $\text{m s}^{-1}$  during the first 12 hours of 13 December, the significant wave height continues to increase. The significant wave height reaches 7.1 m at 2200 UTC when the wind speed is only 4.7  $\text{m s}^{-1}$ . The significant wave height then decreases to 5 m while the wind speed increases to 10  $\text{m s}^{-1}$ .

Figure 8 shows the wave spectra and mean wave direction at two time periods on 12 December when the

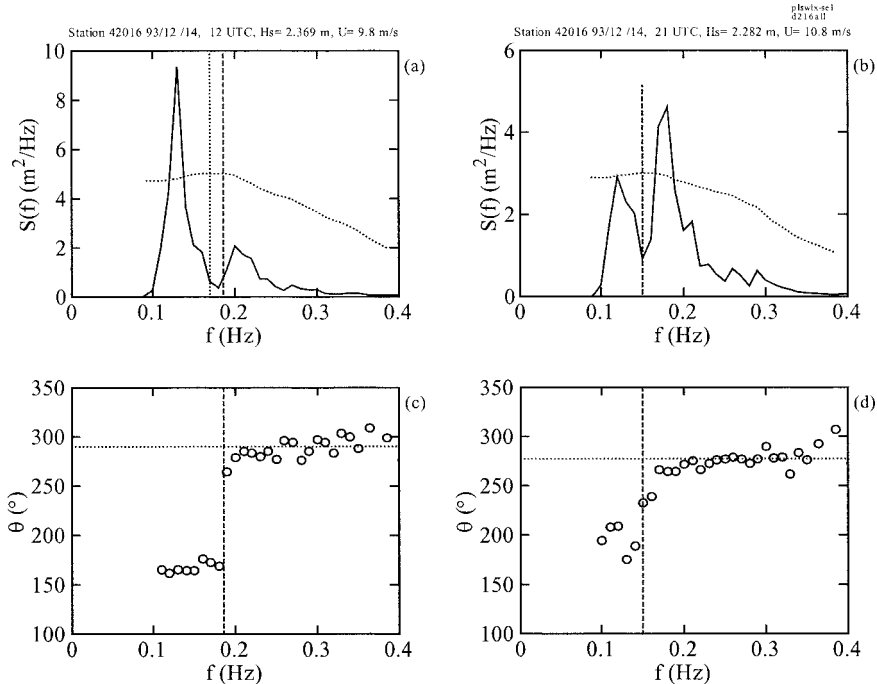


FIG. 6. Same as Fig. 5 at two time periods after the frontal passage. Note that  $f_m$  equals  $f_s$  in (b), which causes the overlap of the vertical dotted and dashed lines.

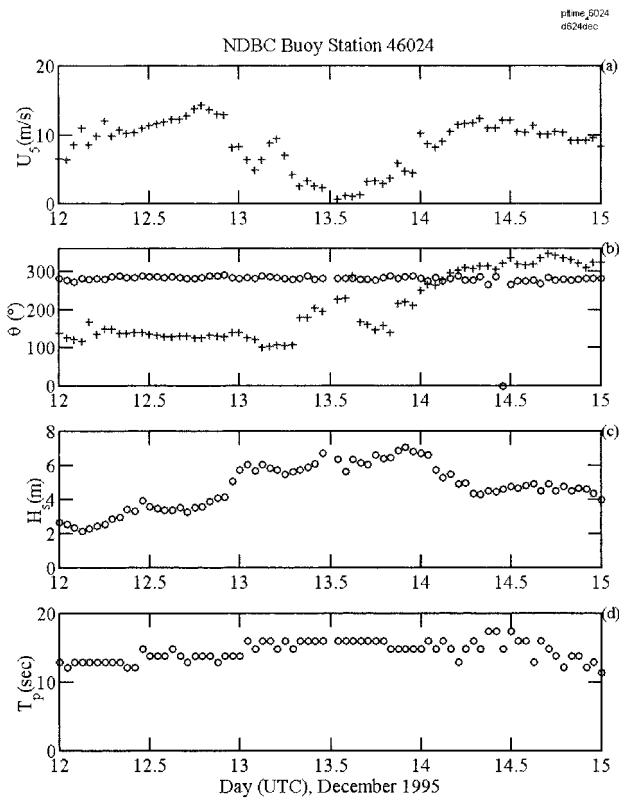


FIG. 7. Time history of hourly measured (a) wind speed, (b) wind direction (crosses) and dominant wave direction (circles), (c) significant wave height, and (d) peak wave period during the period of 12–14 Dec 1995 from the offshore buoy off the California coast (ID 46024).

wind sea generated by the southeasterly wind (horizontal dotted lines in Figs. 8c and 8d) coexists with the dominant westerly swell. Also shown are their associated steepness functions (dotted lines in Figs. 8a and 8b). The spectra display a major low-frequency energy peak around 0.07 Hz with a direction of about 280° and a secondary high-frequency peak associated with the southeasterly wind sea. In spite of the presence of the strong westerly swell in the spectra, the steepness functions remain smooth and single peaked with its peak frequency closer to the spectral peak of the southeasterly wind sea. The separation frequency of the steepness method (vertical dashed lines) is located between the wind sea and swell peaks. The mean wave directions at frequencies lower than the separation frequency are mainly in the westerly wind direction. The mean wave directions at frequencies higher the separation frequency align into the prevailing southeasterly wind direction. It is noted that the high-frequency waves of wind sea are about 20° more southerly than the wind direction. The larger difference between wind and wave directions may be attributed to the slant fetch effect, which occurs when the offshore wind blows at an oblique angle to the shoreline orientation producing asymmetric fetch conditions with respect to the wind direction. As a result, the dominant waves are aligned more from the direction of longer fetch, instead of following the wind direction (Donelan et al. 1985; Walsh et al. 1989).

Figure 9 shows wave spectra and mean wave directions at two time periods on 14 December when the wind sea generated by the northwesterly wind coexists

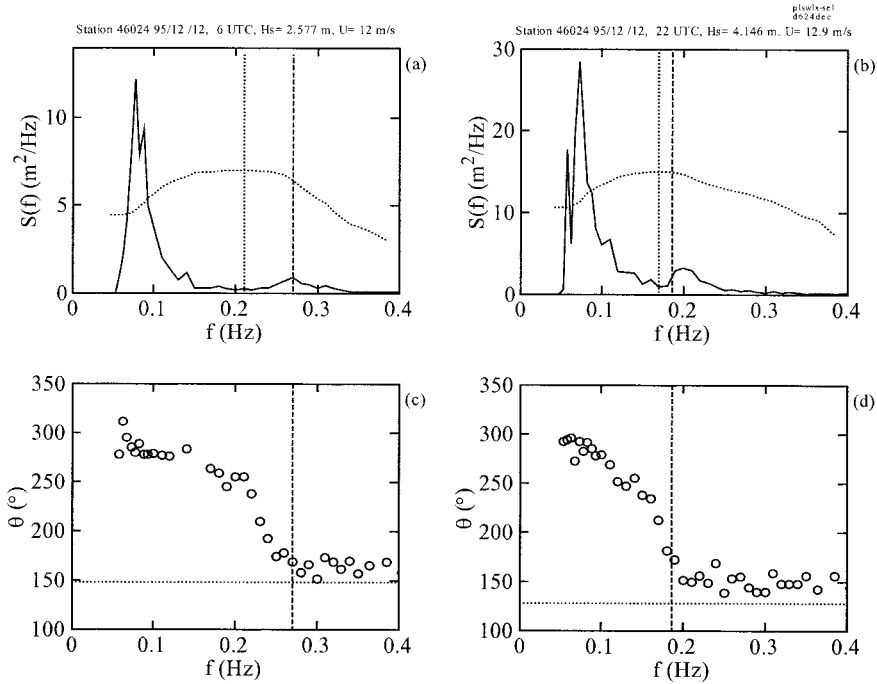


FIG. 8. (a) and (b) Wave spectra and (c) and (d) their frequency-dependent mean wave direction (circles) from the buoy off the California coast at two time periods during the southeasterly wind. The local wind direction is indicated by the horizontal dotted lines in (c) and (d). The dotted lines in (a) and (b) are the scaled steepness function with its peak frequency  $f_m$  indicated by the vertical dotted lines. The vertical dashed line indicates the separation frequency from the steepness method  $f_s$ .

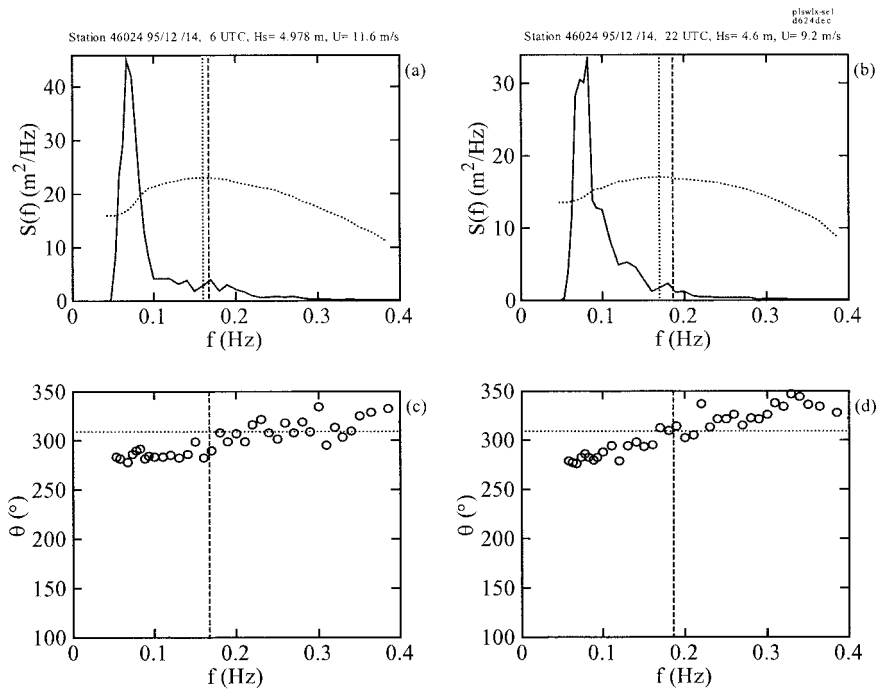


FIG. 9. Same as Fig. 8, at two time periods during the northwesterly winds.

with the westerly swell. The spectra display a very sharp low-frequency peak associated with the westerly swell. The high-frequency energy peak of the wind sea is rather broad and indistinctive. The steepness function (dotted lines in Figs. 9a and 9b) has a smoother shape than the wave spectra with its peak remains at higher frequencies. The mean wave directions at the higher frequencies align with the northwesterly wind direction (horizontal dotted lines) and gradually shift to the westerly swell direction at lower frequencies. The separation frequency of the steepness method (vertical dashed lines) is located at where the mean wave direction starts to deviate from the local northwesterly wind direction into the westerly swell direction. The steepness method shows a proper determination of the separation frequency even when the wind sea and swell are from more or less the same direction and the spectrum has a very indistinctive wind sea peak.

*c. Effects of variability of the separation frequency to energy separation*

The separation frequency from (10) is based on the generalized relations in (8) and (9). The separation frequency represents an average value with statistical variability. Additional variability could also come from the determination of the peak frequency  $f_m$  from a rather flatter top of the steepness function (see Fig. 8a). The effect of the variability to the energy separation of wind sea and swell could vary depending on different spectral shapes for various types of wind sea and swell coexistence. The three spectra shown in Figs. 8b, 6a, and 6b representing three types of wind sea and swell coexistence, which have the ratio of separated swell energy to the total wave energy  $E_s/E$  of 0.83, 0.69, and 0.29, respectively, indicating the sea state from the swell to wind sea dominance. The variability of the separation frequency is simulated by decreasing and increasing the original separation frequency from (10) by 5%, 10%, and 15%. The wind sea and swell energy for the changed separation frequency is then recalculated and compared to that from the original separation frequency. Figure 10a shows the change of swell energy versus the change of separation frequency. The change of swell energy is related to decrease and increase of the separation frequency. For the case with  $E_s/E = 0.69$ , a 15% increase in the separation frequency results in a swell energy increase by about 20%. Very similar results are also observed in the effect of separation frequency variability to the change of wind sea energy (Fig. 10b). In general, for the sea state with a lower  $E_s/E$ , the varying separation frequency causes larger swell energy change and smaller wind sea energy change. It is noted that the above analysis does not address the effect of the separation distance between the wind sea and swell peaks. When there is a larger separation distance with a lower energy trough between the wind sea swell peaks, the

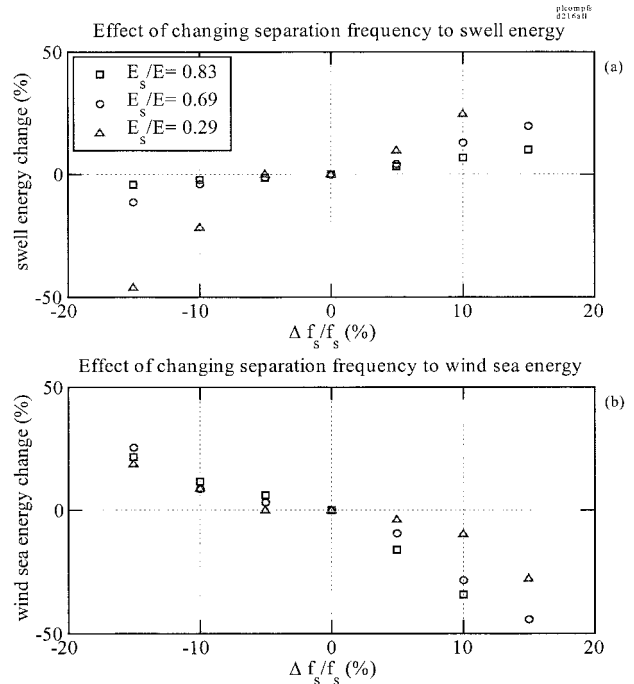


FIG. 10. The change of separation frequency vs the change of (a) swell energy and (b) wind sea energy for  $E_s/E = 0.83$  (squares), 0.69 (circles), and 0.29 (triangles).

impact of separation frequency variability to energy separation should be less.

**4. Representative wave height and wave period of wind sea and swell**

With the use of the separation frequency for a given wave spectrum, the representative wave height and wave period of wind sea and swell components can be calculated separately. The significant wave height  $H_{sw}$ , and average wave period  $T_{zw}$  of the wind sea components are defined as

$$H_{sw} = 4\sqrt{m_{0w}}, \quad \text{and} \quad (11)$$

$$T_{zw} = \sqrt{\frac{m_{0w}}{m_{2w}}}, \quad (12)$$

where  $m_{0w}$  and  $m_{2w}$  are computed from

$$m_{nw} = \int_{f_s}^{f_{max}} f^n S(f) df, \quad n = 0, 2. \quad (13)$$

The significant wave height  $H_{ss}$  and average wave period  $T_{zs}$  of the swell components are defined as

$$H_{ss} = 4\sqrt{m_{0s}}, \quad \text{and} \quad (14)$$

$$T_{zs} = \sqrt{\frac{m_{0s}}{m_{2s}}}, \quad (15)$$

where  $m_{0s}$  and  $m_{2s}$  are computed from

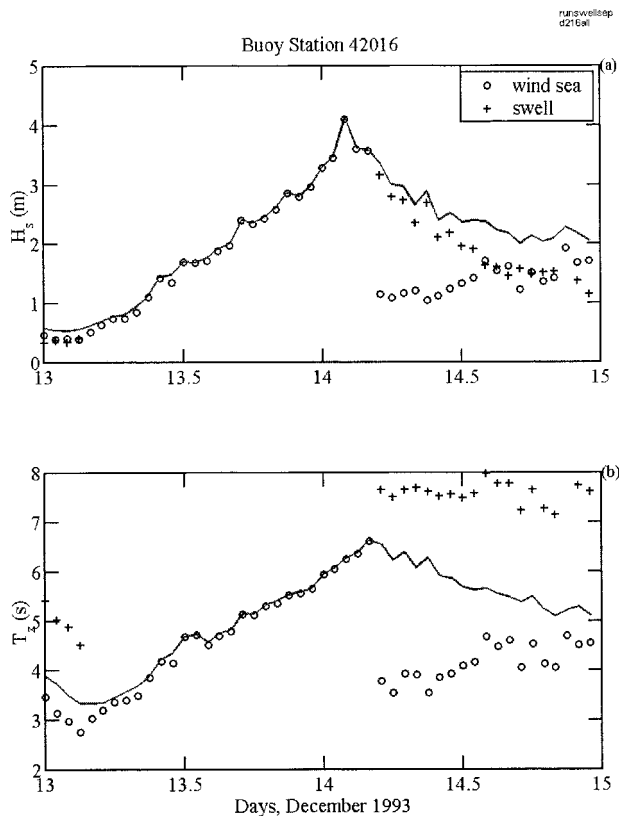


FIG. 11. Time history of the separated (a) significant wave height and (b) average wave period of wind sea (circles) and swell (crosses) during 13–14 Dec 1993 from the offshore buoy in the Gulf of Mexico. The solid lines in (a) and (b) are the buoy-reported significant wave height and average wave period.

$$m_{ns} = \int_{f_{\min}}^{f_s} f^n S(f) df, \quad n = 0, 2. \quad (16)$$

Figure 11 shows the time history of  $H_{sw}$  and  $T_{zw}$  (circles) and  $H_{ss}$  and  $T_{zs}$  (crosses) of the frontal passage case in the Gulf of Mexico. The significant wave height  $H_s$  and average wave period  $T_z$  reported from the NDBC's buoy are also displayed (solid lines). When the sea state is dominated by wind seas prior to the frontal passage,  $H_{sw}$  and  $T_{zw}$  of wind sea are very close to  $H_s$  and  $T_z$ , respectively. After the frontal passage, the separation of wind sea and swell provides a more detailed description of the evolution of the sea state. The gradually decaying sea state is, in fact, a combination of the growing northwesterly wind sea and the decaying southeasterly swell. The  $H_{sw}$  of wind sea gradually increases from about 1.1 to 1.8 m with the  $T_{zw}$  increasing from about 3.5 to 4.5 s, while  $H_{ss}$  of swell gradually drops from about 3 to 1 m with the  $T_{zs}$  varying between 7 and 8 s. Figure 12 shows the time history of  $H_{sw}$  and  $T_{zw}$  (circles) and  $H_{ss}$  and  $T_{zs}$  (crosses) of the offshore California coast case. The buoy-reported significant wave height  $H_s$  and average wave period  $T_z$  are also displayed (solid lines).

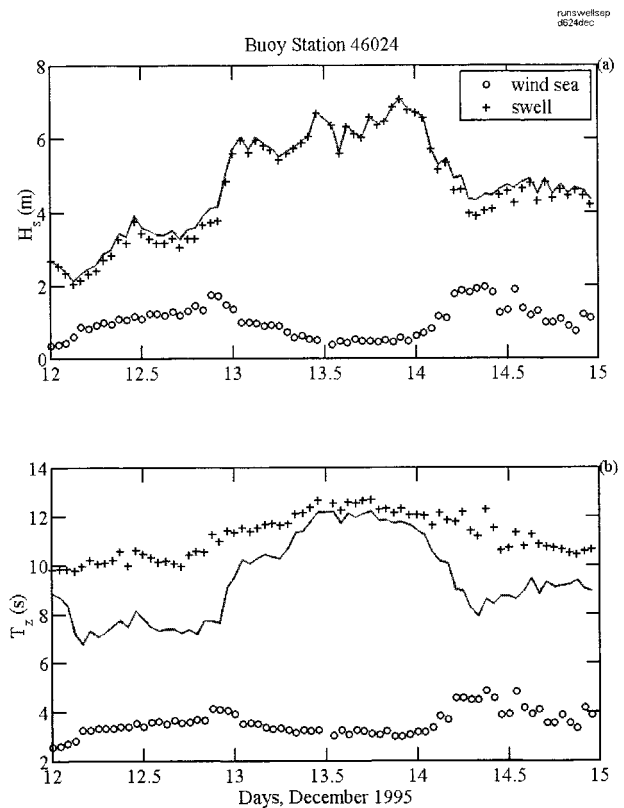


FIG. 12. Same as Fig. 8 during 12–14 Dec 1995 from the offshore buoy off the California coast.

The  $H_{ss}$  of swell is very close to the  $H_s$  as the  $T_{zs}$  of swell varies between 10 and 12 s. The variation of  $H_{sw}$  of wind sea (Fig. 12a) is consistently in phase with that of wind speed (Fig. 7a) as the  $T_{zw}$  of wind sea varies between 3 and 5 s (Fig. 12b).

The relation of the representative wave height and wave period is often used to provide a general depiction of wave climate. Figures 13a and 13b show the buoy-reported significant wave height  $H_s$  versus average wave period  $T_z$  for December 1993 from the buoy in the Gulf of Mexico and for December 1995 from the buoy off the California coast. The separated  $H_{sw}$  versus  $T_{zw}$  of wind sea (circles) and  $H_{ss}$  versus  $T_{zs}$  of swell (crosses) for the two cases are shown in Figs. 13c and 13d, respectively. The dashed lines in the figures represent the relation  $H_s = 0.01gT_z^2$ , which is associated with the global steepness limit of small breaking waves riding on long waves (Xu et al. 1986). Due to the fact that the sea state off the California coast is significantly influenced by the constant arrivals of strong long period swells, the relation of wave height and wave period (Fig. 13b) deviates significantly from the global steepness limit  $H_s = 0.01gT_z^2$  with a much larger data scatter than that in the Gulf of Mexico (Fig. 13a). Using the separation frequency from the steepness method, the relation of wave height and wave period can be studied separately for the wind sea and swell. The relation of  $H_{sw}$

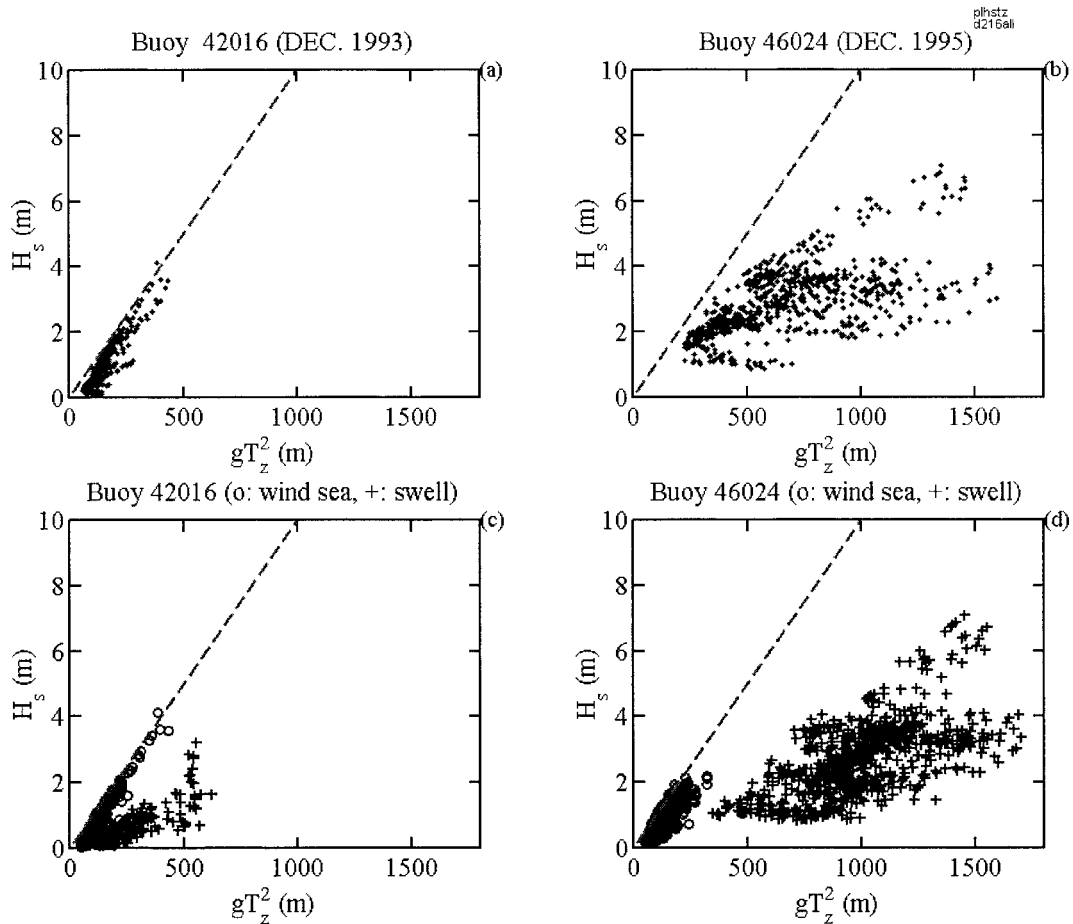


FIG. 13. Scatterplot of the significant wave heights vs average wave periods from the buoys (a) in the Gulf of Mexico for Dec 1993, and (b) off the California coast for Dec 1995. The scatterplot of separated significant wave heights and average wave periods for wind sea (circles) and swell (crosses) during the same period from the two offshore buoys (c) in the Gulf of Mexico and (d) off the California coast. The dashed lines in the figures represent the steepness limit of breaking waves  $H_s = 0.01gT_z^2$  (Xu et al. 1986).

and  $T_{zw}$  of wind sea in the Gulf of Mexico and off the California coast is compactly bounded by the breaking wave steepness limit  $H_s = 0.01gT_z^2$ . The relation of  $H_{ss}$  and  $T_{zs}$  of swell is more variable and deviates significantly from  $H_s = 0.01gT_z^2$ , especially in the data off the California coast that shows a much larger data scatter.

**5. Summary**

Coexistence of wind sea and swell often results in double-peaked or multiple-peaked spectra. Identification and separation of the wave energies of wind sea and swell from the measured spectra allow us to have a more realistic description of the sea state, which is of great practical importance to offshore structure design, safety of marine operation, and the study of wind wave dynamics. This paper describes the development of a physics-based method to determine the separation frequency of wind sea and swell based on the consideration of wave steepness. A frequency-dependent steepness

function representing the average steepness of wave components above a given frequency  $f_*$  is defined in (7). The characteristics of the steepness function are more related to the high-frequency wind sea components and the peak frequency of the steepness function is almost invariant to the presence of low-frequency swell components. Using the Pierson-Moskowitz spectral model for the wind sea spectrum, the separation frequency is derived from the peak frequency of the steepness function. Field tests of the steepness method are conducted using wind and directional wave data from buoys in the Gulf of Mexico and off the California coast. Excellent performance of the steepness method for separating wind sea and swell under various marine weather conditions is demonstrated. The application of the steepness method does not rely on the wind information or directional spectral data and can be easily implemented for operational applications. Examples are given to illustrate the separated characteristics of the relation of wave heights and wave periods for wind sea and swell.

The steepness function involves the use of second moment of the wave spectrum in (7), which could be sensitive to noises appearing at the tail end of the wave spectrum. In practice, a cutoff upper-frequency limit between 0.4 and 0.5 Hz is suggested. Due to the use of the upper-frequency limits, the proposed steepness method may not work well at low wind conditions, especially in the earlier hours of wind wave generation when wind-generated waves have little energy and are at higher frequencies than the chosen upper-frequency limit.

*Acknowledgments.* This work is supported by the Office of Naval Research (Naval Research Laboratory Program Element N62435), "Phase Resolved Nonlinear Transformation of Shoaling Waves."

#### REFERENCES

- Aranuvachapun, S., 1987: Parameters of JONSWAP spectral model for surface gravity waves-II. Predictability from real data. *J. Ocean Eng.*, **14**, 101–115.
- Dobson, F. W., S. D. Smith, and R. J. Anderson, 1994: Measuring the relationship between wind stress and sea state in the open ocean in the presence of swell. *Atmos.–Ocean*, **32**, 237–236.
- Donelan, M. A., W. M. Drennan, and K. B. Katsaros, 1997: The air–sea momentum flux in conditions of wind sea and swell. *J. Phys. Oceanogr.*, **27**, 2087–2099.
- Earle, M. D., 1984: Development of algorithms for separation of sea and swell. National Data Buoy Center Tech. Rep. MEC-87-1, 53 pp.
- Gerling, T. W., 1992: Partitioning sequences and arrays of directional ocean waves spectra into component wave systems. *J. Atmos. Oceanic Technol.*, **9**, 444–458.
- Guedes Soares, C., 1984: Representation of double-peaked sea wave spectra. *J. Ocean Eng.*, **11**, 185–207.
- , 1991: On the occurrence of double-peaked wave spectra. *J. Ocean Eng.*, **18**, 167–171.
- , and M. C. Nolasco, 1992: Spectral modeling of sea states with multiple wave systems. *J. Offshore Mech. Arct. Eng.*, **114**, 278–284.
- Hanson, J. L., 1996: Wave spectral partitioning applied to the analysis of complex wave conditions in the North Pacific Ocean. Preprints, *Eighth Conf. on Air–Sea Interaction and Symp. on Goals*, Atlanta, GA, Amer. Meteor. Soc., 61–65.
- , and O. M. Phillips, 1999: Wind sea growth and dissipation in the open ocean. *J. Phys. Oceanogr.*, **29**, 1633–1648.
- , and —, 2001: Automated analysis of ocean surface directional wave spectra. *J. Atmos. Oceanic Technol.*, **18**, 277–293.
- Huang, N. E., S. R. Long, and L. F. Bliven, 1981: On the importance of the significant slope in empirical wind-wave studies. *J. Phys. Oceanogr.*, **11**, 569–573.
- Kline, S. A., and J. L. Hanson, 1995: Wave identification and tracking system. Applied Physics Laboratory, The Johns Hopkins University, Tech. Rep. STD-R-2436, Laurel, MD, 44 pp.
- Lewis, A. W., and R. N. Allos, 1990: JONSWAP's parameters: Sorting out inconsistencies. *J. Ocean Eng.*, **17**, 409–415.
- Mitsuyasu, H., 1991: The effect of swell on the growth of wind waves. *Oceanography of Asian Marginal Seas*, K. Takano, Ed., Elsevier, 381–391.
- , 1997: On the contribution of swell to sea surface phenomena. *Proc. Seventh Int. Offshore and Polar Engineering Conf.*, Honolulu, HI, Int. Society of Offshore and Polar Engineers, 1–7.
- Pierson, W. J., and L. Moskowitz, 1964: A proposed spectral form for fully developed wind seas based on the similarity theory of S. A. Kitaigorodskii. *J. Geophys. Res.*, **69**, 5181–5190.
- Rodriguez, C., and C. Guedes Soares, 1999: A criterion of the automatic identification of multimodal sea wave spectra. *Appl. Ocean Res.*, **21**, 329–333.
- Steele, K. E., and T. Mettlach, 1993: NDBC wave data-current and planned. *Proc. Second Int. Symp. on Ocean Wave Measurement and Analysis*, New Orleans, LA, ASCE, 198–207.
- , C. C. Teng, and D. W. Wang, 1992: Wave direction measurements using pitch-roll buoys. *J. Ocean Eng.*, **19**, 349–375.
- Tucker, M. J., 1991: *Waves in Ocean Engineering: Measurement, Analysis, Interpretation*. Ellis Horwood Ltd., 431 pp.
- Vartdal, L., and S. F. Barstow, 1987: A separation algorithm for wind sea and swell for applications to directional Metocean data buoy. Oceanographic Center, SINTEF Group Tech. Rep. ANODA-30, Trondheim, Norway, 104 pp.
- The WAMDI Group, 1988: The WAM model—A third generation ocean wave prediction model. *J. Phys. Oceanogr.*, **18**, 1775–1810.
- Walsh, E. J., D. W. Hancock, D. E. Hines, R. N. Swift, and J. F. Scott, 1989: An observation of the directional wave spectrum evolution from shoreline to fully developed. *J. Phys. Oceanogr.*, **19**, 670–690.
- Xu, D., P. A. Hwang, and J. Wu, 1986: Breaking of wind-generated waves. *J. Phys. Oceanogr.*, **16**, 2172–2178.